

# Cell Method Analysis of Crack Propagation in Tensioned Concrete Plates

E. Ferretti<sup>1</sup>

**Abstract:** In this study, the problem of finding the complete trajectory of propagation and the limiting load in plates with internal straight cracks is extended to the non-linear field. In particular, results concerning concrete plates in bi-axial tensile loading are shown. The concrete constitutive law adopted for this purpose is monotonic non-decreasing, as following according to previous studies of the author on monotonic mono-axial loading. The analysis is performed in a discrete form, by means of the Cell Method (CM). The aim of this study is both to test the new concrete constitutive law in biaxial tensile load and to verify the applicability of the CM in crack propagation problems for bodies of non-linear material. The discrete analysis allows us to identify the crack initiation without using the stress intensity factors.

**Keywords:** non-linear analysis, concrete, crack initiation, crack trajectory, Cell Method.

## 1 Introduction

For finding the crack trajectory and the minimum load required to propagate a crack (limiting load), the variational principle of the most common crack theories has been used over the past years [Patron and Morozov (1978)]. Criteria for the initiation of crack propagation can be obtained on the basis of both energy and force considerations. Historically, at first an energy fracture criterion was proposed by A. A. Griffith in 1920 [Griffith (1920)] and G. R. Irwin formulated a force criterion in 1957 [Irwin (1957, 1958)], while the same time demonstrating the equivalence of the two criteria. Griffith, Inglis (1913) and Irwin developed the foundations of linear elastic fracture mechanics.

The Irwin force criterion for crack extension and the equivalent Griffith energy criterion completely solve the question of the limiting equilibrium state of a cracked

---

<sup>1</sup> DISTART, Scienza delle Costruzioni, Facoltà di Ingegneria, Alma Mater Studiorum, Università di Bologna, Viale Risorgimento 2, 40136 (BO), Italy.

continuous elastic body. Nevertheless, there exists a number of other formulations also establishing the limiting equilibrium state of a cracked body. Among these, the best known models are those of Leonov and Panasyuk [Leonov and Panasyuk (1959)], Dugdale [Dugdale (1960)], Wells [Wells (1961)], Novozhilov [Novozhilov (1969)], and McClintock [McClintock (1958)]. Detailed introductions into linear elastic fracture mechanics can be found in Heckel (1983), Anderson (1991), Rolfe and Barsom (1987) and Broek (1974).

Sneddon found approximate results for the stress distribution at the crack tip for the first time [Sneddon (1975)]. Rice and Rosengren (1968) and Hutchinson (1968) developed solutions for the stress field considering plastic deformations in the crack tip region [Koenke et al. (1998)]. The stress intensity factor (SIF) is one of the most important parameters in Fracture Mechanics in order to properly define the stress field close to the crack tip. Paris and Sih [Paris and Sih (1965)] have collected a number of solutions in a comprehensive handbook for the three basic modes of SIF, namely  $K_I$   $K_{II}$   $K_{III}$ , for varying crack sizes and relatively simple-shaped structures. For the more realistic complex shapes encountered in practice, the finite element method (FEM) is widely used for the evaluation of the stress intensity factors for mode I II and III for various types of crack configurations and for the solution of both linear elastic and elasto-plastic fracture problems [Souiyah et al. (2009)]. With the FEM the stresses are computed from the displacements solution, the primary output of the FE codes, by means of extrapolation techniques. Besides the classical FEM, various other numerical methods have been used to derive SIFs, such as Enriched Finite Element Method, deformed Finite Element Method, Finite Difference Method (FDM), Boundary Element Method (BEM) and energy-based methods like J-integral, energy release and stiffness derivative methods. Several numerical analyses of cracks of different shapes have been performed in past years in order to evaluate SIFs [Bowie (1956), Newman (1971), Owen (1973), Hellen (1975), Murakami (1978), Chang (1981), De Araújo et al. (2000), Gustavo, Jaime and Manuel (2000), Yan (2006), Abdelaziz, Abou-bekr and Hamouine (2007), Al-shoaibi, Hadi and Ariffin (2007), Aour, Rahmani and Nait-Abdelaziz (2007), Kutuka, Atmacab and Guzelbey (2007), Laurencin, Delette and Dupeux (2007), Shihani and Tabatabaei (2008), Stanislav and Zdenek (2008)].

Three prevalent theories have been developed for the determination of the angle at which a crack would propagate under mixed mode loading conditions. The first theory, introduced by Erdogan and Sih [Erdogan and Sih (1963)], postulates that the crack will propagate in the direction normal to the radial line for which the hoop stress at the crack tip becomes maximum. In the general case of loading by mode I and II, the angle  $\vartheta_0$  of crack extension measured from the tip of the crack with reference to the line to which the straight crack belongs (axis  $x'$  in Fig. 1),

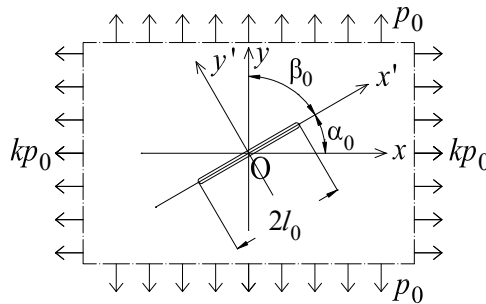


Figure 1: Load and geometrical set-up of the cracked plate

with  $\vartheta_0$  counterclockwise positive, is given in terms of  $K_I$  and  $K_{II}$  by means of the relationship:

$$\vartheta_0 = \text{asin} \left[ K_{II} \frac{K_I \pm 3\sqrt{K_I^2 + 8K_{II}^2}}{K_I^2 + 9K_{II}^2} \right], \tag{1}$$

which is the solution of the following equation:

$$K_I \sin \vartheta_0 + K_{II} (3 \cos \vartheta_0 - 1) = 0. \tag{2}$$

According to the second theory, developed by Sih [Sih, (1974)], the crack will propagate in the direction along which the strain energy density possesses a stationary (minimum) value while, according to the third theory, developed by Hussain [Hussain Pu and Underwood (1974)], the parameter to predict the incipient crack turning angle is the maximum energy release rate.

In Fracture Mechanics, the variational problem of finding the limiting load and the correlated crack propagation direction is reduced to that of finding extreme points of a function of several variables [Patron and Morozov (1978)]. In the present paper, the variational approach has been abandoned in favor of a discrete formulation of the crack propagation problem based on the Cell Method (CM) [Tonti (2001a)]. The use of a discrete formulation instead of a variational one is advantageous, since it does not require the definition of a model for treating the zone ahead of the crack edge. When studying crack problems for an elastic-perfectly plastic body with the energy equilibrium criterion, for instance, the solution is usually given in the case when the plastic deformation is concentrated in a narrow zone ahead of the crack edge. The thickness of this zone is of the order of elastic displacements. Moreover, when the plastic zone ahead of the edge is thin, the problem is reduced to

the solution of an elastic problem instead of an elastic-plastic one. This reduction is based on the fact that, in the linearized formulation, a thin plastic zone may be schematically replaced by an additional cut along the face of which are applied forces replacing the action of the plastically deforming material. Attention is then drawn to the fact that the region of plastic non-linear effects in the model under consideration varies with the external load and represents a plastically deforming material in which the state of stress and strain must be determined from the solution of an elastic-plastic problem. With the discrete formulation, on the contrary, no hypothesis on the shape and dimensions of the plastic zone is needed, and the calculation is performed directly, without having to reduce the problem to an equivalent elastic one.

## 2 Theoretical basics of the Cell Method

The Cell Method (CM) is a new numerical method for solving field equations [Tonti (2001a)], aiming at providing a direct finite formulation of field equations, without requiring a differential formulation (Fig. 2). The theoretical basics of the CM consist in highlighting the geometrical, algebraic and analytical structure which is common to different physical theories [Tonti (2001a), Ferretti (2005)]. This leads to a unified description of Physics and allows for using the CM for the solution of problems in different fields of physics science and engineering, such as acoustics [Tonti (2001b)], electrostatics [Bettini and Trevisan (2003), Marrone (2004), Heshmatzadeh and Bridges (2007)], magnetostatics [Alotto and Perugia (2004), Marrone (2004), Trevisan and Kettunen (2004), Alotto et al. (2006), Giuffrida Grusso and Repetto (2006)], Eddy currents [Specogna and Trevisan (2005), Alotto et al. (2008), Codecasa Specogna and Trevisan (2008)], electromagnetism in the time-domain [Marrone and Mitra (2004)] and in the frequency-domain [Marrone Grassi and Mitra (2004)], elastostatics [Cosmi (2001), Tonti and Zarantonello (2009)], fracture mechanics [Ferretti (2003), Ferretti (2004a), Ferretti (2004c), Ferretti (2005), Ferretti and Di Leo (2003), Ferretti Casadio and Di Leo (2008)], elastodynamics [Cosmi (2005), Cosmi (2008)] and fluid dynamics [Straface Troisi and Gagliardi (2006)]. The CM has been also applied to thermal conduction [Bullo et al. (2006) Bullo et al. (2007)], diffusion [Bottauscio et al. (2004)], biomechanics [Cosmi and Dreossi (2007), Taddei et al. (2008), Cosmi et al. (2009)], heterogeneous materials modeling [Ferretti (2005), Ferretti Casadio and Di Leo (2008)], mechanics of porous materials [Cosmi (2003), Cosmi and Di Marino (2001)] and structural mechanics [Nappi and Tin-Loi (2001), Ferretti Casadio and Di Leo (2008)] problems.

As far as the common geometrical structure is concerned, the fundamental observation on which the CM is built is that the geometrical referent of the physical vari-

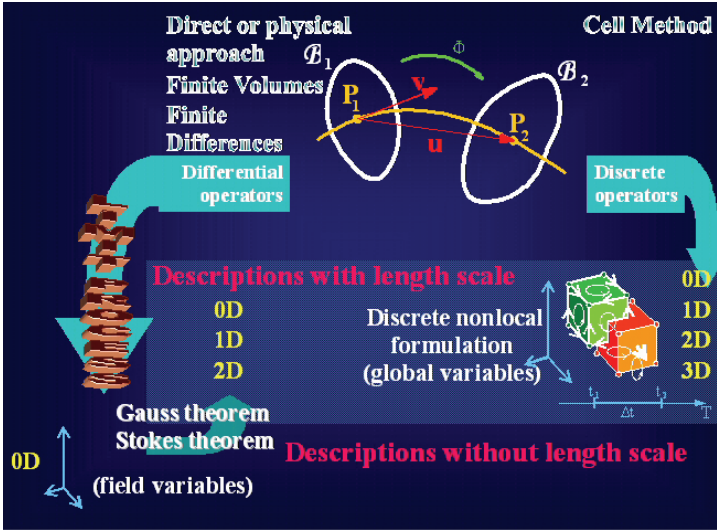


Figure 2: How to achieve the solution through the Cell Method, a truly discrete formulation, and the methods for which the discrete formulation is induced by the differential formulation

ables of any physical theory, which are global variables, is not necessarily a point. The physical variables are also associated to lines (voltage, stretching, velocity circulation), surfaces (charge flow, discharge, heat, surface force), and volumes (mass content, momentum content). This put the limit process of the differential formulation – whose effect consists in reducing the global variables to field variables defined in the point by performing densities and rates – under discussion from the physical point of view. The CM relates the physical variables to their geometrical referent directly by associating them to the nodes, edges, surfaces and volumes of two cell complexes, in dual relationship by each other (Fig. 2) and not to the points of a coordinate system, as one does for the differential formulation.

As discussed in Ferretti (2005), the main difference between the differential and the discrete approaches concerns the nonlocal description of the continuum. The different description of nonlocality comes just from performing (differential approach) or not performing (CM) the limit process. Since in the first case the global variables are reduced to point (and instant) variables, the metrics is lost and must be reintroduced a-posteriori, by means of a length scale, if one wants to describe the nonlocal effects. This also happens for the direct or physical approach, the vertex-

based scheme of the Finite Volume Method, and the Finite Differences Method. Both could be considered very similar to the CM while they start from point-wise conservation equations and derive the discrete formulation by the differential formulation (Fig. 2). With the CM, oppositely, we do not need to recover the length scale since it is preserved by avoiding the limit process (Fig. 2). As a consequence, the CM allows for obtaining a nonlocal formulation by using local constitutive laws.

Recently, Heshmatzadeh and Bridges (2007) have compared in detail CM and FEM in electrostatics, proving the equivalence of the coefficient matrices for a Voronoi dual mesh and linear shape functions in the FEM, also showing that the use of linear shape functions in FEM is equivalent to the use of a barycentric dual mesh for charge vectors.

The numerical code for crack trajectory analysis with the CM has been developed by the author [Ferretti (2003, 2008)]. In this study, the code has been extended to provide results in the case of a concrete plate tensioned at infinity by a load of intensity  $p_x = kp_0$  parallel to the  $x$ -axis and  $p_y = p_0$  parallel to the  $y$ -axis (Fig. 1). The plate has an initial straight crack of length  $2l_0$  oriented at an angle  $\alpha_0$  to the  $x$ -axis ( $\beta_0$  to the  $y$ -axis). The crack trajectory and the minimum load required to propagate the crack from the ends of the cut are provided for various values of  $k$  and  $\alpha_0$ .

### 3 Crack extension criterion

The minimum load required to propagate a crack (limiting load) can be deduced by using a variety of criteria:

- maximal normal stress criterion;
- maximal strain criterion;
- minimum strain energy density fracture criterion;
- maximal strain energy release rate criterion;
- damage law criteria.

In the present paper, the crack extension condition is studied in the Mohr-Coulomb plane. The limiting load is computed as the load satisfying the condition of tangency between the Mohr's circle representing the stress field in the neighborhood of the tip and the Leon limit surface (Fig. 3). With  $c$  being the cohesion,  $f_c$  the compressive strength,  $f_{tb}$  the tensile strength,  $\tau_n$  and  $\sigma_n$ , respectively, the shear

and normal stress on the attitude of external normal  $n$ , the Leon criterion in the Mohr-Coulomb plane is expressed as:

$$\tau_n^2 = \frac{c}{f_c} \left( \frac{f_{tb}}{f_c} + \sigma_n \right). \tag{3}$$

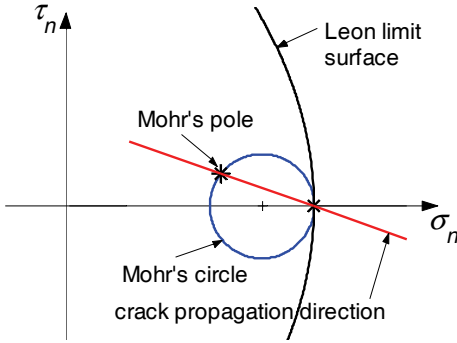


Figure 3: Leon limit surface

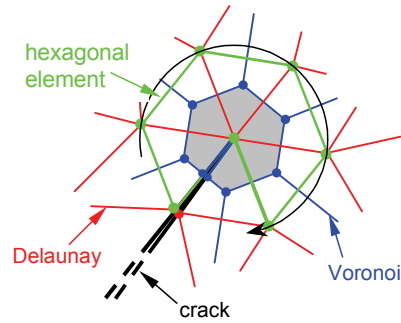


Figure 4: Hexagonal element for stress analysis at the crack tip

The Mohr's circle for the tip neighborhood is identified by means of the physical significance associated with the CM domain discretization: the CM divides the domain by means of two cell complexes, in such a way that each cell of the first cell complex, which is a simplicial complex, contains one, and one only, node of the second cell complex (in this study, a Delaunay/Voronoi mesh generator is used to generate the two meshes in two-dimensional domains). The primal mesh (the Delaunay mesh) is obtained by subdividing the domain into triangles, so that for each triangle of the triangulation the circumcircle of that triangle is empty of all other sites (Fig. 4). The dual mesh (the Voronoi mesh) is formed by the polygons whose vertexes are at the circumcenters of the primal mesh (Fig. 4). For each Voronoi site, every point in the region around that site is closer to that site than to any of the other Voronoi sites. Now, the conservation law is enforced on the dual polygon of every primal vertex [Ferretti (2003)] and the stresses are computed on the nodes of the dual mesh. Thus, not only the displacements, like in the FEM, but also the stresses are primary outputs of a CM code and it is no longer necessary to use point matching techniques to determine stresses and SIFs. The crack propagation direction is then derived in the Mohr/Coulomb plane directly as the line joining the Mohr's pole to the point in which the circle of Mohr is tangent to the limit surface. In effect, both lines joining one of the two tangent points at the limiting stage to

the Mohr's pole identify propagation directions. For the plate in Fig. 1, due to the biaxial state of tensile stress at the ends of the cut, the Mohr's circle of the attitudes making bundle around the  $z$ -axis is fully contained in the positive half-plane of the normal stress. It follows that the Mohr's circle at the limiting stage is tangent to the limit surface of Leon in just one point, the vertex of the parabola of Leon (Fig. 3). Consequently, just one propagation direction activates at each stage of the propagation process.

In order to identify the Mohr's circle for the tip neighborhood, a hexagonal element has been inserted at the tip ([Ferretti (2003)], Fig. 4). When the mesh generator is activated, the hexagonal element is divided into equilateral Delaunay triangles and a quasi-regular tip Voronoi cell is generated (the cell filled in gray in Fig. 4). This allows us to establish a correspondence between the tip stress field and the attitudes corresponding to the sites of the tip Voronoi cell. It has been shown [Ferretti (2003)] that the tension points correctly describe the Mohr's circle in the Mohr-Coulomb plane, for rotation of the hexagonal element around the tip.

The used crack propagation technique is the intra-element technique with nodal relaxation and subsequent re-meshing. Extension of this technique to the activation of two propagation directions is provided in Ferretti (2008) even for the case in which crack bifurcation occurs during propagation.

#### 4 Constitutive Assumption

The concrete constitutive law adopted in this study is monotonic non-decreasing, in accordance with the identification procedure for concrete in mono-axial load provided in Ferretti (2005) (Fig. 5). It was shown [Ferretti (2004b, 2005)] how this constitutive law turned out to be size insensitive for mono-axial compressive load. This result has made it possible to formulate a new concrete law in mono-axial loading, the effective law, which can be considered more representative of the material physical properties than the softening laws are. Now, the effective law is tested for applications in bi-axial tensile load. The tensile branch has been here identified starting from the compressive one, in the assumption that a homothetic relationship exists between the two branches (Fig. 5). A ratio between tensile and compressive strength of  $1/12$ ,  $1/8$ ,  $1/6$ ,  $1/4$ ,  $1/3$  and  $1/2$  has been considered. The best accordance between analytical and experimental results has been obtained for the ratio equal to  $1/8$ .

#### 5 Parametric analysis of the limiting load

Numerical results concerning the limiting load for the concrete plate loaded as shown in Fig. 1 are here presented. For symbols and conventions, refer to Fig. 1.

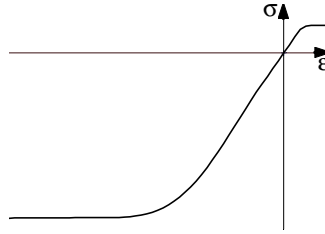


Figure 5: Adopted constitutive law for concrete in mono-axial load

The  $p_y$  mapping for  $k = 0$  and  $\alpha_0 = \pi/4$ , plotted on the deformed configuration of a finite area around the crack, is shown in Fig. 6 for the initial straight crack. In this figure, the darker red color corresponds to the maximal tensile stress, while the darker green color corresponds to the value  $p_y = 0$ .

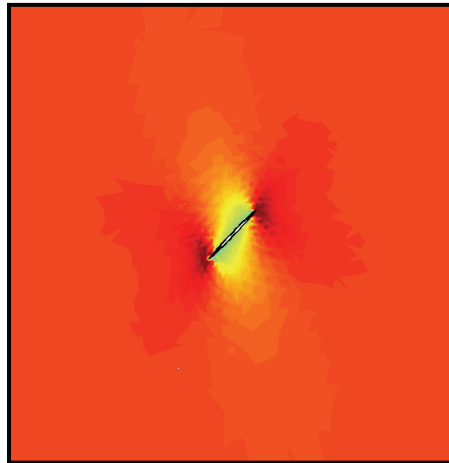


Figure 6: 2D  $p_y$  mapping for the initial straight crack with  $k = 0$ ,  $\alpha_0 = \pi/4$

In Fig. 7, the  $p_y$  mapping is provided in 3D, with the level lines plotted also in the neutral plane,  $p_y = 0$ . The significance of colors is the same as in Fig. 6. The 3D plot correctly shows how  $p_y$  reaches a value numerically close to 0 near the crack boundary. The boxed area in the plane  $p_y = 0$  of Fig. 7 is the plot area of Fig. 6. As all the level lines are internal to the boxed area, it can be assumed with good approximation that this area represents the stress extinction zone for the initial straight crack.

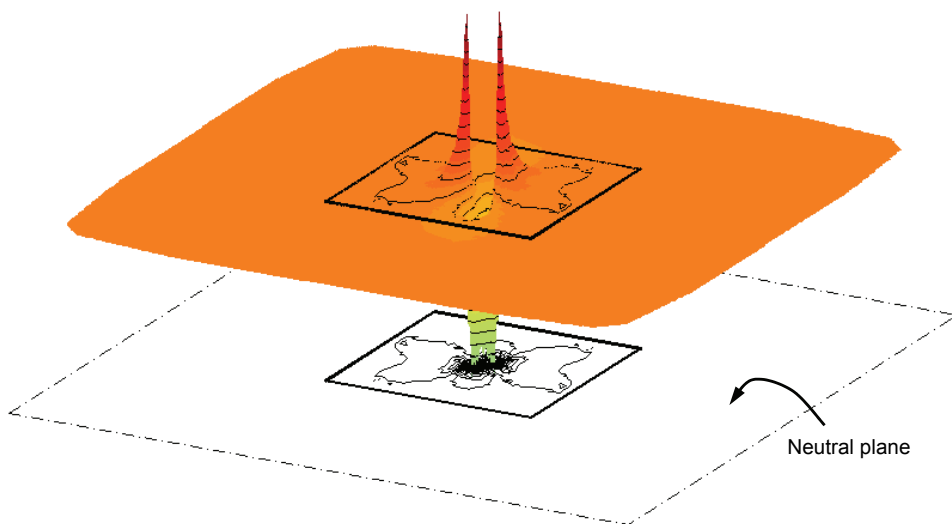


Figure 7: 3D  $p_y$  mapping and lines of equal  $p_y$  for the initial straight crack with  $k = 0$ ,  $\alpha_0 = \pi/4$

The normalized limiting load in the direction of the  $y$ -axis for a prefixed value of the load ratio  $k$ :

$$\bar{p}_{y_{lim}}(\alpha_0, k)|_{k=const} = \frac{p_{y_{lim}}(\alpha_0, k)|_{k=const}}{p_{y_{max}}}, \quad (4)$$

with:

$$p_{y_{max}} = \max_{\alpha_0, k} p_{y_{lim}}(\alpha_0, k), \quad (5)$$

is plotted in Fig. 8 in function of the angle  $\alpha_0$  (or, which is the same, in function of  $\beta_0 = \pi/2 - \alpha_0$ ) for the factor  $k$  equal to 0, 1/4, 1/2, 3/4 and 1. The figure exhibits a  $\bar{p}_{y_{lim}}$  limiting load increasing with  $\alpha_0$  for each constant value of  $k$  in the field  $0 \leq k < 1$ , stating that the value  $\alpha_0 = 0$  gives the critical crack orientation for all the biaxial load conditions, the  $x$ -component being lower than the  $y$ -component. The constant behavior of the relationship obtained for  $k = 1$  is in good agreement with the homogeneous state of stress represented by this load condition. In this case, all the crack orientations to the  $x$ -axis return the same limiting load.

The limiting load  $p_{y_{lim}}$  for a given load ratio  $k = \bar{k}$  and a given crack inclination  $\alpha_0 = \bar{\alpha}_0$  is the same as the limiting load  $p_{x_{lim}}$  for the reciprocal load ratio  $k = 1/\bar{k}$

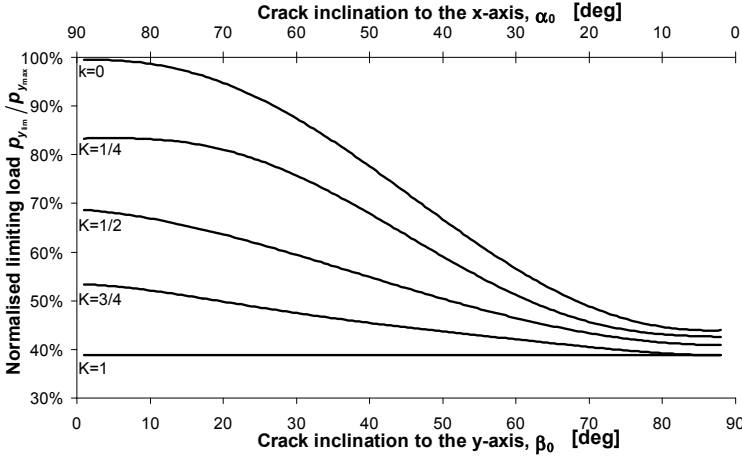


Figure 8: Normalized limiting load  $\bar{p}_{y_{lim}}$  in function of the crack inclinations  $\alpha_0$  and  $\beta_0$  for  $0 \leq k \leq 1$

and the complementary crack inclination  $\beta_0 = \bar{\alpha}_0$ . By defining the ideal limiting load  $p_{id_{lim}}$  as:

$$p_{id_{lim}} = \sqrt{p_{x_{lim}}^2 + p_{y_{lim}}^2} = p_{0_{lim}} \sqrt{k^2 + 1}, \quad (6)$$

it follows that  $p_{id_{lim}}$  assumes the same values for load conditions and crack inclinations which both are symmetric with respect to the bisector of the first quadrant,  $y = x$ , with  $x$  and  $y$  the axes in Fig. 1.

The line  $y = x$  superimposes to the crack when the crack is oriented at the angle  $\alpha_0 = \pi/4$  (or, which is the same, at the angle  $\beta_0 = \pi/4$ ). Thus, in the plane  $\alpha_0/p_{id_{lim}}$  (or  $\beta_0/p_{id_{lim}}$ ) the curves of the ideal limiting load for the given value  $\bar{k}$  of  $k$  and its reciprocal value  $k = 1/\bar{k}$  are symmetric with respect to the line  $\alpha_0 = \pi/4$  (or  $\beta_0 = \pi/4$ ).

In Fig. 9, the curves of the normalized ideal limiting load for a prefixed value of the load ratio  $k$ :

$$\bar{p}_{id_{lim}}(\alpha_0, k)|_{k=const} = \frac{p_{id_{lim}}(\alpha_0, k)|_{k=const}}{p_{id_{max}}}, \quad (7)$$

with:

$$p_{id_{max}} = \max_{\alpha_0, k} p_{id_{lim}}(\alpha_0, k), \quad (8)$$

are plotted in function of the angles  $\alpha_0$  and  $\beta_0$  for the load factor  $k$  equal to  $\bar{k} = 0, 1/4, 1/2, 3/4, 1$  (solid lines) and its reciprocal values  $k = 1/\bar{k} = \infty, 4, 2, 4/3, 1$  (dotted lines). Even in the plane  $\alpha_0/\bar{p}_{id_{lim}}(\beta_0/\bar{p}_{id_{lim}})$ , each couple of  $\bar{p}_{id_{lim}}$  curves plotted for reciprocal values of the load factor,  $k = \bar{k}$  and  $k = 1/\bar{k}$ , are symmetric with respect to the line  $\alpha_0 = \beta_0 = \pi/4$  (Fig. 9), of course. Each curve in Fig. 9 represents the function:

$$f_k = f_k(\alpha_0) = \bar{p}_{id_{lim}}(\alpha_0, k)|_{k=\bar{k}}, \quad 0 \leq \alpha_0 \leq \frac{\pi}{2} \tag{9}$$

returning the relationship between  $\bar{p}_{id_{lim}}$  and  $\alpha_0$  at the given value  $\bar{k}$  of  $k$ . The locus of the  $f_k$  curves for the whole range of variability of the load factor,  $0 \leq k \leq +\infty$ , is the function of two variables:

$$\Omega = \Omega(\alpha_0, k) = \bar{p}_{id_{lim}}(\alpha_0, k) \quad 0 \leq \alpha_0 \leq \frac{\pi}{2}, \quad 0 \leq k \leq \infty, \tag{10}$$

which is a surface of the space of axes  $\alpha_0, k$  and  $\bar{p}_{id_{lim}}$  defining the value of normalized ideal limiting load in function of the crack orientation and the ratio between the loads in direction of the  $x$ - and  $y$ -axis.

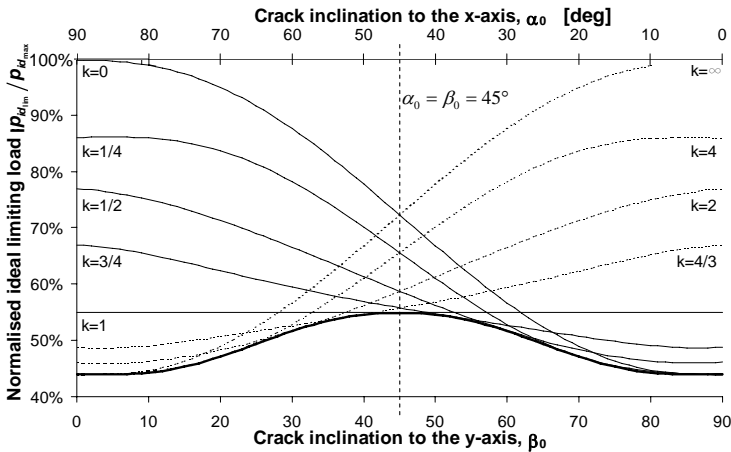


Figure 9: Normalized ideal limiting load  $\bar{p}_{id_{lim}}$  in function of the crack inclinations  $\alpha_0$  and  $\beta_0$  for  $0 \leq k \leq +\infty$

The thick line in Fig. 9, lower envelope of the  $f_k$  curves in the plane  $\alpha_0/\bar{p}_{id_{lim}}$  (or  $\beta_0/\bar{p}_{id_{lim}}$ ), is the plot of the function  $w_{\alpha_0 k}$ :

$$w_{\alpha_0 k} = w_{\alpha_0 k}(\alpha_0) = \min_{\substack{\alpha_0 = \bar{\alpha}_0 \\ 0 \leq k \leq \infty}} \Omega(\alpha_0, k) = \min_{\substack{\alpha_0 = \bar{\alpha}_0 \\ 0 \leq k \leq \infty}} \bar{p}_{id_{lim}}(\alpha_0, k), \tag{11}$$

with:

$$0 \leq \alpha_0 \leq \frac{\pi}{2}. \tag{12}$$

Each point of the function (11) is obtained for different values of the load factor  $k$  and, thus, belongs to different  $f_k$  curves. Consequently,  $w_{\alpha_0 k}$  is the projection on the plane  $\alpha_0/\bar{p}_{id_{lim}}$  (or  $\beta_0/\bar{p}_{id_{lim}}$ ) of a 3D function of the space of axes  $\alpha_0$ ,  $k$  and  $\bar{p}_{id_{lim}}$ , named  $\omega_{\alpha_0}$ , where  $\alpha_0$  and  $k$  are not independent variables since they are bonded by the condition (11) of minimum load. Said  $k_{lim}^{cr} = k_{lim}^{cr}(\alpha_0)$  the load factor providing the minimum value of normalized ideal limiting load  $\bar{p}_{id_{lim}}$  for each assigned  $\alpha_0 = \bar{\alpha}_0$ :

$$k_{lim}^{cr}(\alpha_0) = k : \bar{p}_{id_{lim}}|_{\substack{\alpha_0=\bar{\alpha}_0 \\ k=k_{lim}^{cr}}} = \min_{\substack{\alpha_0=\bar{\alpha}_0 \\ 0 \leq k \leq \infty}} \bar{p}_{id_{lim}}(\alpha_0, k), \quad 0 \leq \alpha_0 \leq \frac{\pi}{2} \tag{13}$$

the function  $\omega_{\alpha_0}$  returning the minimum  $\bar{p}_{id_{lim}}$  for a given  $\alpha_0 = \bar{\alpha}_0$  and  $0 \leq k \leq +\infty$  can be written as:

$$\omega_{\alpha_0} = \omega_{\alpha_0}(\alpha_0, k_{lim}^{cr}) = \min_{\substack{\alpha_0=\bar{\alpha}_0 \\ 0 \leq k \leq \infty}} \Omega(\alpha_0, k) = \min_{\substack{\alpha_0=\bar{\alpha}_0 \\ 0 \leq k \leq \infty}} \bar{p}_{id_{lim}}(\alpha_0, k), \tag{14}$$

with:

$$0 \leq \alpha_0 \leq \frac{\pi}{2}. \tag{15}$$

The function (13), where  $k_{lim}^{cr}$  is the ratio between  $p_x^{cr}$  and  $p_y^{cr}$  at the limit state, is provided by the projection of  $\omega_{\alpha_0}$  on the plane  $\alpha_0/k$ , said  $w_{\alpha_0 p}$  (Fig. 10):

$$w_{\alpha_0 p} = w_{\alpha_0 p}(\alpha_0) = k_{lim}^{cr}(\alpha_0). \tag{16}$$

$k_{lim}^{cr}$  can be also expressed as the solution of the following differential problem:

$$k_{lim}^{cr} = k_{lim}^{cr}(\alpha_0) = k : \left. \frac{\partial \bar{p}_{id_{lim}}(\alpha_0, k)}{\partial k} \right|_{\substack{\alpha_0=\bar{\alpha}_0 \\ k=k_{lim}^{cr}}} = 0, \quad \left. \frac{\partial^2 \bar{p}_{id_{lim}}(\alpha_0, k)}{\partial k^2} \right|_{\substack{\alpha_0=\bar{\alpha}_0 \\ k=k_{lim}^{cr}}} > 0 \tag{17}$$

In the aim to plot the 3D surface of the normalized ideal limiting load given by Eq. (10) for the whole range of variability of the load factor,  $0 \leq k \leq +\infty$ , the second independent variable of  $\Omega$ ,  $k$ , has been substituted by the variable  $\psi$  defined as follows:

$$\psi = \psi(k) = 1 - e^{-k}, \quad 0 \leq k \leq +\infty. \tag{18}$$

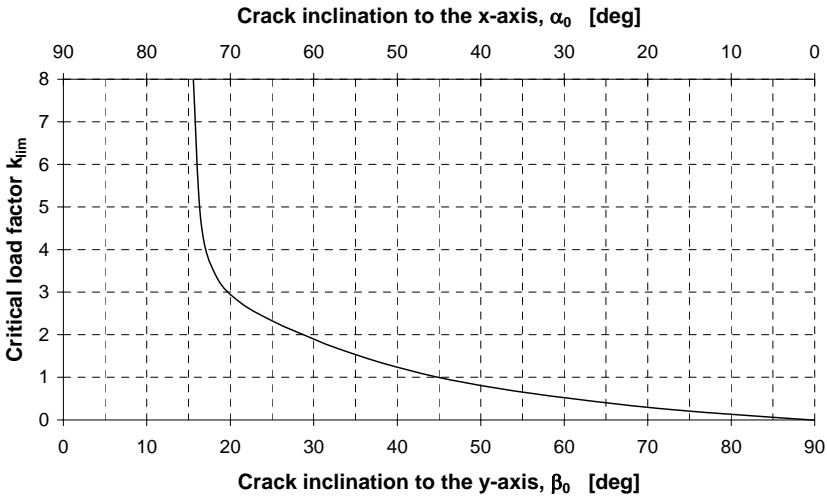


Figure 10: Load factor  $k_{lim}^{CR}$  providing the minimum value of  $\bar{p}_{id_{lim}}$  for each assigned  $\alpha_0 = \bar{\alpha}_0$

With the change of variable (18), the surface of the normalized ideal limiting load is given by the function:

$$\hat{\Omega} = \hat{\Omega}(\alpha_0, \psi) = \bar{p}_{id_{lim}}(\alpha_0, \psi), \quad 0 \leq \alpha_0 \leq \frac{\pi}{2}, \quad 0 \leq \psi \leq 1, \tag{19}$$

which substitutes Eq. (10). The Eq. (19) gives a finite 3D representation of  $\bar{p}_{id}$ , in function of  $\alpha_0$  (or  $\beta_0$ ) and  $\psi$ , since the ranges of variability of its independent variables are finite ranges (Eq. (19)).

Some plots of  $\hat{\Omega}$  obtained for different axes orientation are given in Fig. 11. In particular, Fig. 11.a is the 3D equivalent representation of Fig. 9. Each line in Fig. 11.a represents the function:

$$\hat{f}_{\psi} = \hat{f}_{\psi}(\alpha_0) = \bar{p}_{id_{lim}}(\alpha_0, \psi)|_{\psi=\bar{\psi}}, \quad 0 \leq \alpha_0 \leq \frac{\pi}{2}, \tag{20}$$

returning the relationship between  $\bar{p}_{id_{lim}}$  and  $\alpha_0$  at the given value  $\bar{\psi}$  of  $\psi$ . Since the difference between the two surfaces  $\Omega$  and  $\hat{\Omega}$  stands in the change of the variable plotted along the axis which is orthogonal both to the planes of Fig. 9 and Fig. 11.a (Eq. (18)), it follows that the plot of the function  $f_k$  is equal to that of the function  $\hat{f}_{\psi}$ :

$$f_k(\alpha_0)|_{k=\bar{k}} = \hat{f}_{\psi}(\alpha_0)|_{\psi=\bar{\psi}=1-e^{-\bar{k}}}, \quad 0 \leq \alpha_0 \leq \frac{\pi}{2}. \tag{21}$$

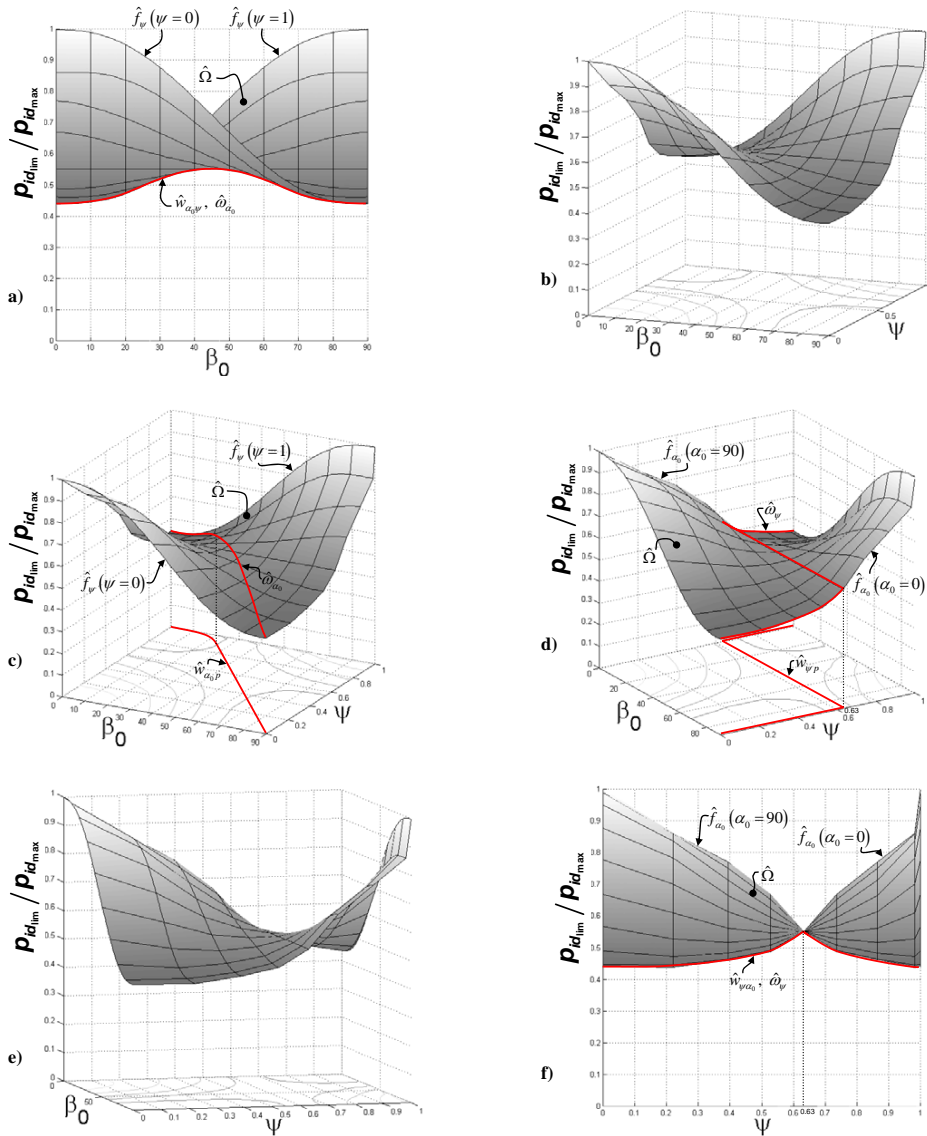


Figure 11: Some examples of finite 3D representation of  $\bar{P}_{id,lim}$ , in function of  $\beta_0$  and  $\psi$

The lower envelope of the  $\hat{f}_\psi$  curves in the plane  $\alpha_0/\bar{p}_{id_{lim}}$  (or  $\beta_0/\bar{p}_{id_{lim}}$ ) is the function  $\hat{w}_{\alpha_0\psi}$  (Fig. 11.a):

$$\hat{w}_{\alpha_0\psi} = \hat{w}_{\alpha_0\psi}(\alpha_0) = \min_{\substack{\alpha_0=\bar{\alpha}_0 \\ 0 \leq \psi \leq 1}} \hat{\Omega}(\alpha_0, \psi) = \min_{\substack{\alpha_0=\bar{\alpha}_0 \\ 0 \leq \psi \leq 1}} \bar{p}_{id_{lim}}(\alpha_0, \psi), \quad (22)$$

with:

$$0 \leq \alpha_0 \leq \frac{\pi}{2}. \quad (23)$$

Once more, from Eq. (18) it follows that:

$$w_{\alpha_0 k}(\alpha_0)|_{k=\hat{k}} = \hat{w}_{\alpha_0\psi}(\alpha_0) |_{\psi=\hat{\psi}=1-e^{-\hat{k}}}, \quad 0 \leq \alpha_0 \leq \frac{\pi}{2}. \quad (24)$$

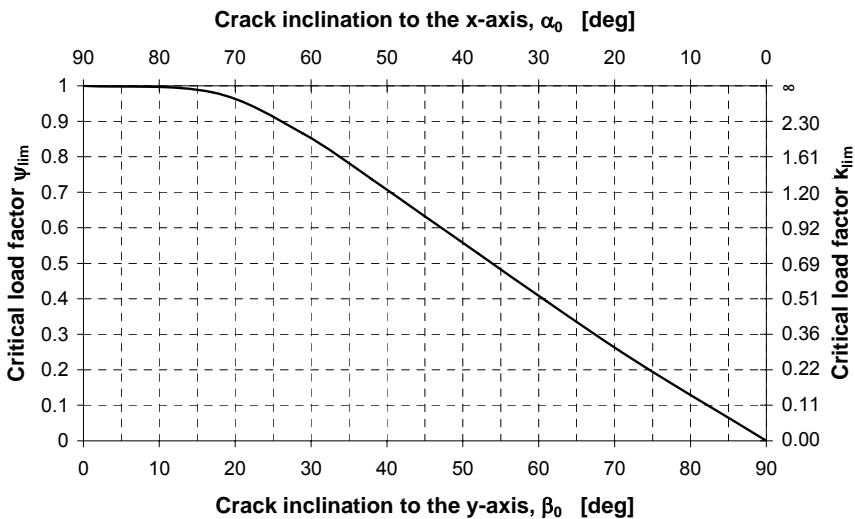


Figure 12: Load factors  $\psi_{lim}^{cr}$  and  $k_{lim}^{cr}$  providing the minimum value of  $\bar{p}_{id_{lim}}$  for each assigned  $\alpha_0 = \bar{\alpha}_0$

$\hat{w}_{\alpha_0\psi}$  is the projection on the plane  $\alpha_0/\bar{p}_{id_{lim}}$  (or  $\beta_0/\bar{p}_{id_{lim}}$ ) of the 3D function  $\hat{w}_{\alpha_0}$  of the space of axes  $\alpha_0$ ,  $\psi$  and  $\bar{p}_{id_{lim}}$  ( Fig. 11.a,c), with  $\alpha_0$  and  $\psi$  bonded by the condition (22) of minimum  $\bar{p}_{id_{lim}}$ . Said  $\psi_{lim}^{cr} = \psi_{lim}^{cr}(\alpha_0)$  the value of  $\psi$  providing the minimum value of normalized ideal limiting load  $\bar{p}_{id_{lim}}$  for a given  $\alpha_0 = \bar{\alpha}_0$ :

$$\psi_{lim}^{cr}(\alpha_0) = \psi : \bar{p}_{id_{lim}}|_{\alpha_0=\bar{\alpha}_0} = \min_{\substack{\alpha_0=\bar{\alpha}_0 \\ 0 \leq \psi \leq 1}} \bar{p}_{id_{lim}}(\alpha_0, \psi), \quad 0 \leq \alpha_0 \leq \frac{\pi}{2} \quad (25)$$

the function  $\hat{\omega}_{\alpha_0}$  can be written as:

$$\hat{\omega}_{\alpha_0} = \hat{\omega}_{\alpha_0}(\alpha_0, \psi_{\text{lim}}^{cr}) = \min_{\substack{\alpha_0 = \bar{\alpha}_0 \\ 0 \leq \psi \leq 1}} \hat{\Omega}(\alpha_0, \psi) = \min_{\substack{\alpha_0 = \bar{\alpha}_0 \\ 0 \leq \psi \leq 1}} \bar{p}_{id_{\text{lim}}}(\alpha_0, \psi), \quad (26)$$

with:

$$0 \leq \alpha_0 \leq \frac{\pi}{2}. \quad (27)$$

The projection of the function  $\hat{\omega}_{\alpha_0}$  on the plane  $\alpha_0/\psi$ , named  $\hat{w}_{\alpha_0 p}$  in Fig. 11.c, returns the relationship between  $\psi_{\text{lim}}^{cr}$  and  $\alpha_0$  (Fig. 12):

$$\hat{w}_{\alpha_0 p} = \hat{w}_{\alpha_0 p}(\alpha_0) = \psi_{\text{lim}}^{cr}(\alpha_0). \quad (28)$$

In Fig. 12 also the axis of the load factor  $k_{\text{lim}}^{cr}$  is plotted in order to make it possible to evaluate the effect of the change of variable (18) on the law of the minimum  $\bar{p}_{id_{\text{lim}}}$ , by comparing the two functions given by Eqs. 16, plotted in Fig. 10, and 28, plotted in Fig. 12.

The function  $\psi_{\text{lim}}^{cr}$  can be also expressed as the solution of the following differential problem:

$$\psi_{\text{lim}}^{cr} = \psi_{\text{lim}}^{cr}(\alpha_0) = \psi : \left. \frac{\partial \bar{p}_{id_{\text{lim}}}(\alpha_0, \psi)}{\partial \psi} \right|_{\substack{\alpha_0 = \bar{\alpha}_0 \\ \psi = \psi_{\text{lim}}^{cr}}} = 0, \quad \left. \frac{\partial^2 \bar{p}_{id_{\text{lim}}}(\alpha_0, \psi)}{\partial \psi^2} \right|_{\substack{\alpha_0 = \bar{\alpha}_0 \\ \psi = \psi_{\text{lim}}^{cr}}} > 0 \quad (29)$$

The Fig. 11.f is obtained by a 90° rotation of the  $\hat{\Omega}$  surface around the  $\bar{p}_{id}$ -axis. This last plot represents the locus of the functions:

$$\hat{f}_{\alpha_0} = \hat{f}_{\alpha_0}(\psi) = \bar{p}_{id_{\text{lim}}}(\alpha_0, \psi)|_{\alpha_0 = \bar{\alpha}_0}, \quad 0 \leq \psi \leq 1 \quad (30)$$

returning the relationship between  $\bar{p}_{id_{\text{lim}}}$  and  $\psi$  for each assigned value  $\bar{\alpha}_0$  of  $\alpha_0$ . The functions  $\hat{f}_{\alpha_0}$  are the meridians of the surface in Fig. 11.f.

The lower envelope of the  $\hat{f}_{\alpha_0}$  functions gives the function (Fig. 11.f):

$$\hat{w}_{\psi \alpha_0} = \hat{w}_{\psi \alpha_0}(\psi) = \min_{\substack{0 \leq \alpha_0 \leq \frac{\pi}{2} \\ \psi = \bar{\psi}}} \hat{\Omega}(\alpha_0, \psi) = \min_{\substack{0 \leq \alpha_0 \leq \frac{\pi}{2} \\ \psi = \bar{\psi}}} \bar{p}_{id_{\text{lim}}}(\alpha_0, \psi), \quad (31)$$

with:

$$0 \leq \psi \leq 1. \quad (32)$$

$\hat{w}_{\psi\alpha_0}$  is the projection on the plane  $\psi/\bar{p}_{id_{lim}}$  of the 3D function  $\hat{w}_{\psi}$  plotted in Figs. 11.d,f:

$$\hat{w}_{\psi} = \hat{w}_{\psi}(\alpha_0^{cr}, \psi) = \min_{\substack{0 \leq \alpha_0 \leq \frac{\pi}{2} \\ \psi = \bar{\psi}}} \hat{\Omega}(\alpha_0, \psi) = \min_{\substack{0 \leq \alpha_0 \leq \frac{\pi}{2} \\ \psi = \bar{\psi}}} \bar{p}_{id_{lim}}(\alpha_0, \psi), \quad (33)$$

where:

$$\alpha_0^{cr} = \alpha_0^{cr}(\psi) = \alpha_0 : \bar{p}_{id_{lim}}|_{\alpha_0 = \alpha_0^{cr}} = \min_{\substack{0 \leq \alpha_0 \leq \frac{\pi}{2} \\ \psi = \bar{\psi}}} \bar{p}_{id_{lim}}(\alpha_0, \psi), \quad 0 \leq \psi \leq 1 \quad (34)$$

is the crack inclination minimizing the normalized ideal limiting load  $\bar{p}_{id_{lim}}$  for each assigned load factor  $\psi = \bar{\psi}$ . That is to say, as for  $\omega_{\alpha_0}$  and  $\hat{w}_{\alpha_0}$  also the two variables of  $\hat{w}_{\psi}$  are bonded by a condition of minimum load.  $\alpha_0^{cr}$  is the solution of the following differential problem:

$$\alpha_0^{cr} = \alpha_0^{cr}(\psi) = \alpha_0 : \left. \frac{\partial \bar{p}_{id_{lim}}(\alpha_0, \psi)}{\partial \alpha_0} \right|_{\substack{\alpha_0 = \alpha_0^{cr} \\ \psi = \bar{\psi}}} = 0, \quad \left. \frac{\partial^2 \bar{p}_{id_{lim}}(\alpha_0, \psi)}{\partial \alpha_0^2} \right|_{\substack{\alpha_0 = \alpha_0^{cr} \\ \psi = \bar{\psi}}} > 0 \quad (35)$$

As can be seen in Fig. 11.f, all the  $\hat{f}_{\alpha_0}$  functions intersect in one point, of first coordinate:

$$\psi = 1 - \frac{1}{e} \cong 0.63. \quad (36)$$

From Eqs. (36) and (18) it follows that the intersection point of all the  $\hat{f}_{\alpha_0}$  functions is found for the value of the load ratio:

$$k = -\log(1 - \psi) = 1. \quad (37)$$

Since the  $\hat{f}_{\alpha_0}$  functions do not have any other point in common, the  $\alpha_0 = \alpha_0^{cr}$  minimizing  $\bar{p}_{id_{lim}}$  at a given  $\psi$  turns out to be equal to:

$$\alpha_0^{cr} = \begin{cases} 0 & 0 \leq \psi < 1 - \frac{1}{e}, \quad 0 \leq k < 1 \\ [0, \frac{\pi}{2}] & \psi = 1 - \frac{1}{e}, \quad k = 1 \\ \frac{\pi}{2} & 1 - \frac{1}{e} < \psi \leq 1, \quad 1 < k \leq +\infty \end{cases} \quad (38)$$

which means that, as already observed in Fig. 8:

$$\alpha_0^{cr} = \begin{cases} 0 & p_x < p_y \\ [0, \pi/2] & p_x = p_y \\ \pi/2 & p_x > p_y \end{cases} \quad (39)$$

Eq. (38), gives the values of the function  $\hat{w}_{\psi p}$ , projection of  $\hat{w}_{\psi}$  on the plane  $\psi/\alpha_0$  (Fig. 11.d):

$$\hat{w}_{\psi p} = \hat{w}_{\psi p}(\psi) = \alpha_0^{cr}(\psi). \tag{40}$$

The two functions  $\hat{w}_{\alpha_0}$  and  $\hat{w}_{\psi}$  have just one point in common (Fig. 11.c,d), the point for which both functions are stationary:

$$\alpha_0 = \beta_0 = \frac{\pi}{4}, \quad \psi = 1 - \frac{1}{e}. \tag{41}$$

Actually, in a point in which both functions are stationary, looking for the minimum  $\bar{p}_{id_{lim}}$  at constant  $\alpha_0$  is equal to looking for the minimum  $\bar{p}_{id_{lim}}$  at constant  $\psi$ :

$$\min_{\substack{\alpha_0 = \frac{\pi}{4} \\ 0 \leq \psi \leq 1}} \bar{p}_{id_{lim}}(\alpha_0, \psi) = \min_{\substack{0 \leq \alpha_0 \leq \frac{\pi}{2} \\ \psi = 1 - \frac{1}{e}}} \bar{p}_{id_{lim}}(\alpha_0, \psi) = \min_{\substack{0 \leq \alpha_0 \leq \frac{\pi}{2} \\ k=1}} \bar{p}_{id_{lim}}(\alpha_0, k). \tag{42}$$

### 6 Parametric analysis of the propagation path

In Fig. 13 and Fig. 14, the 2D and 3D  $p_y$  analysis for  $k = 0$  and  $\alpha_0 = \pi/4$  is shown for a generic crack propagation step. The lighter colors of Figs. 13 and 14 with respect to those of Figs. 6 and 7 are representative of the progressive plate downloading corresponding to the crack propagation. For the same reason, the values in the third axis of Fig. 14 are smaller than those of Fig. 7. Moreover, in Fig. 13 it can be observed how a mono-axial compressive state of stress of small entity (cyan color) arises in the plate, due to the geometrical effect of the non-straight crack deformation in Mode I.

The crack trajectory is plotted in Fig. 15 for the value of the angle  $\alpha_0$  equal to  $\pi/6$ ,  $\pi/4$  and  $\pi/3$ , and for the factor  $k$  equal to 0, 1/4, 1/2, 3/4 and 1. In this figure, also the two meshes of Delaunay-Voronoi were plotted for  $k = 0$ , in order to show how the adaptive mesh generator recreates the meshes for a generic crack propagation step (Delaunay mesh in red and Voronoi mesh in blue, as indicated in Fig. 4). Fig. 15 shows that the crack trajectory tends to approach an asymptote perpendicular to the external tensile load for all the three cases with  $k = 0$ . The asymptotic behavior is also evident for  $k > 0$ , but the asymptote is now oriented at an angle  $\gamma$  to the  $x$ -axis which depends on  $k$ :

$$\gamma = f(k). \tag{43}$$

The angle  $\gamma$  does not depend on the inclination  $\alpha_0$  of the initial straight crack, since the crack tends to propagate perpendicularly to the tensile principal direction of the

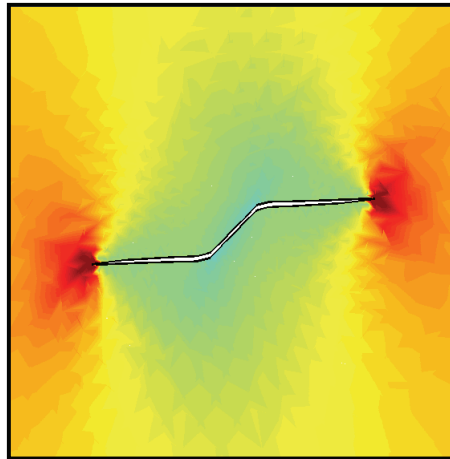


Figure 13: 2D  $p_y$  mapping for a generic propagation step with  $k = 0$ ,  $\alpha_0 = \pi/4$

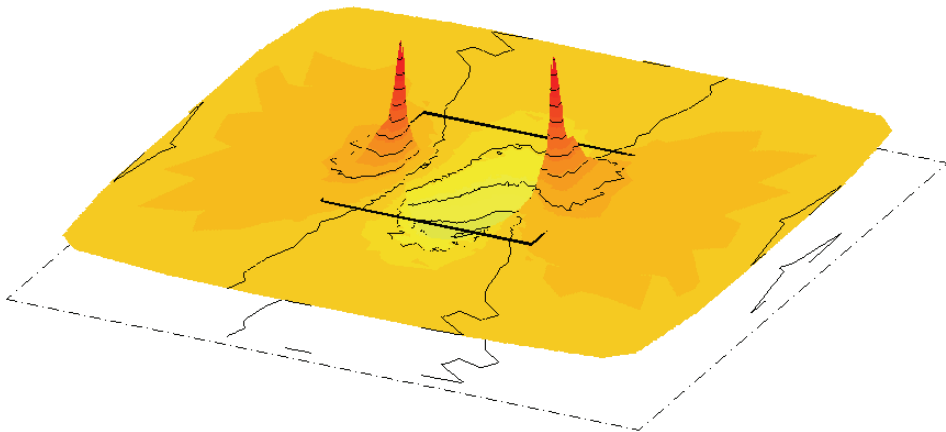


Figure 14: 3D  $p_y$  mapping and lines of equal  $p_y$  for a generic propagation step with  $k = 0$ ,  $\alpha_0 = \pi/4$

uncracked plate. For  $k = 1$ , the angle  $\gamma$  assumes the value  $\pi/4$ , in good accordance with the homogeneous state of stress represented by this load condition:

$$\gamma|_{k=1} = \frac{\pi}{4}. \tag{44}$$

The plot of the function  $\gamma = f(k)$  is provided in Fig. 16 for the range of values

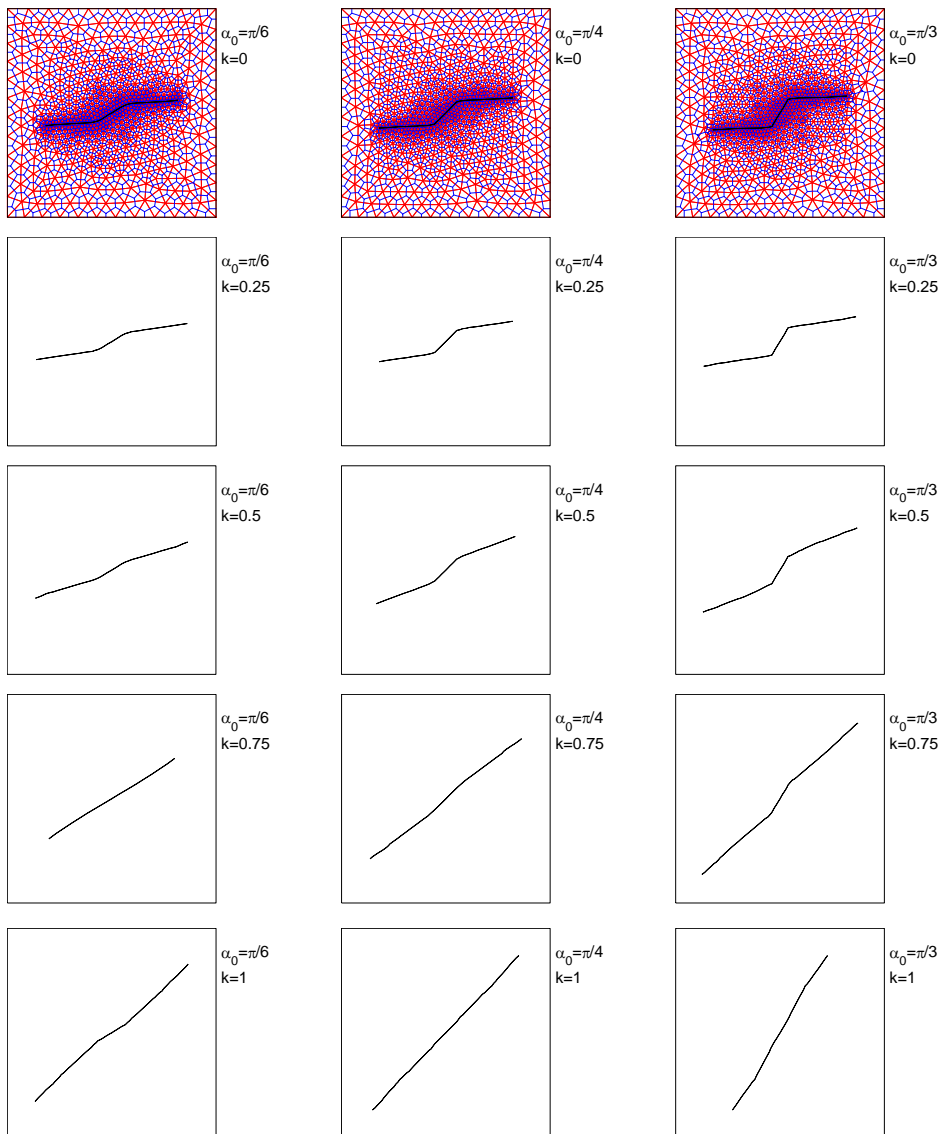


Figure 15: Crack trajectory for  $\alpha_0 = \pi/6, \pi/4, \pi/3$ , and  $k = 0, 1/4, 1/2, 3/4, 1$

$0 \leq k \leq 1$ . The plot of  $\gamma$  for the complete range of values  $0 \leq k \leq +\infty$  (Fig. 17) can be provided by means of the change of variable given by Eq. (18).

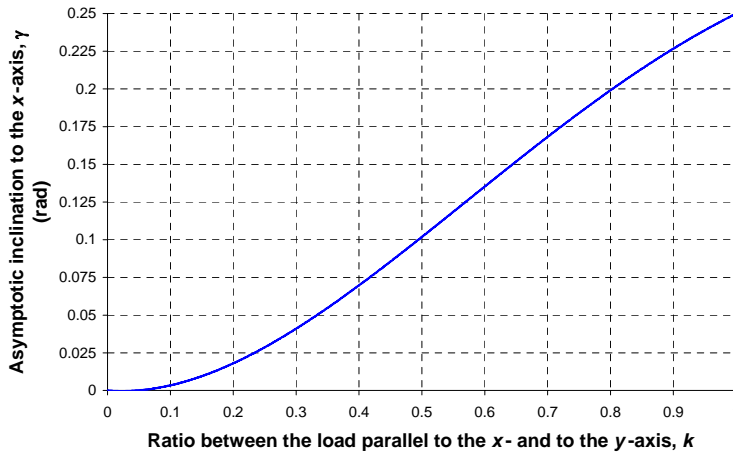


Figure 16: Relationship between the angle  $\gamma$  and the load ratio  $k$

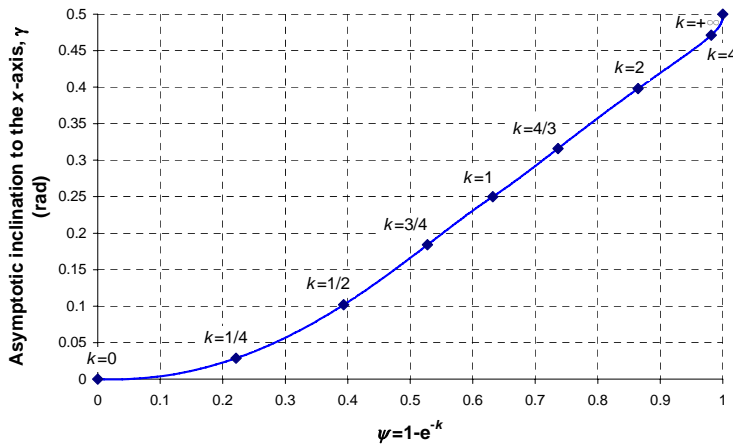
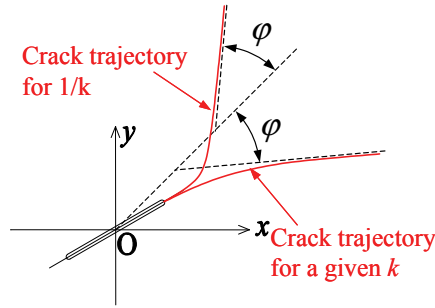


Figure 17: Relationship between the angle  $\gamma$  and the variable  $\psi$

If the behavior of the function  $\gamma = f(k)$  for  $0 \leq k \leq 1$  is known, the behavior of  $\gamma = f(k)$  for  $1 < k \leq +\infty$  is also known. Actually, the asymptotes of the crack trajectory for a given  $k$  and its reciprocal value,  $1/k$ , are symmetric with respect to the bisector of the first quadrant in Fig. 1,  $y = x$  (Fig. 18). That is to say, the value

Figure 18: Crack trajectories for a given  $k$  and  $1/k$ 

assumed by  $\gamma$  for a given  $k$  is equal to the complementary angle of  $\gamma$  for  $1/k$ :

$$\gamma\left(\frac{1}{k}\right) = \frac{\pi}{2} - \gamma(k). \quad (45)$$

Naming  $\varphi$  the clockwise positive angle in Fig. 18, with:

$$\varphi = \frac{\pi}{4} - \gamma, \quad (46)$$

from Eqs. 45 and 46, it follows that:

$$\varphi\left(\frac{1}{k}\right) = -\varphi(k). \quad (47)$$

## 7 Conclusions

A first study on tensioned concrete plates was presented, based on an innovative size-insensitive constitutive law.

The numerical model adopted, based on the CM, allows analysis in the discrete. The crack propagation is then studied without using the stress intensity factors and without having to define a model to treat the zone ahead of the crack tip. This allows one to employ the same numerical code for bodies of different dimensions, geometries and boundary conditions, and for materials of different constitutive laws. As an example of the code versatility in front of the geometrical set-up, the interaction between two or more cracks oriented at any inclination and propagating in plate of finite/infinite dimensions can be easily investigated. As far as the versatility in front of the constitutive law is concerned, the numerical analysis can be indifferently performed in the linear and non-linear field, with no adjunctive computational burdens.

The stress intensity factors of the variational approach can be estimated a-posteriori, since the code allows us to evaluate the compliance decrement following from crack propagation. A comparison between the variational and discrete formulation is then possible, and it will be investigated in future studies.

In this paper, it was shown how the numerical results for plates in bi-axial loading are satisfactory with respect to the load and geometrical parameters.

The crack trajectory exhibits an asymptotic behavior which only depends on the ratio between the load parallel to the  $x$ - and the  $y$ -axis,  $k$ , being insensitive to the inclination  $\alpha_0$  of the initial straight crack. The crack always tends to propagate perpendicularly to the tensile principal direction of the uncracked plate. The numerical law of the asymptotic inclination, said  $\gamma = f(k)$ , was provided for the complete variability range of  $k$ ,  $k = [0, +\infty]$ .

The plausibility of the founded crack trajectories in dependence on the parameter  $k$  indirectly gives a validation of the adopted constitutive law for bi-axial tensile loading.

It was also shown how the numerical crack trajectory for a solid of finite dimensions is highly accurate.

Finally, it is remarkable how the analysis for finite solids is performed directly, without having to apply corrective factors to the solution on an infinite geometry in the same load conditions.

**Acknowledgement:** This work was made possible by the Italian Ministry for Universities and Scientific and Technological Research (MURST).

## 8 References

**Abdelaziz, Y.; Abou-bekr, N.; Hamouine, A.** (2007): Numerical Modeling of the Crack Tip Singularity. *Int. J. Mater. Sci.*, vol. 2, pp. 65-72.

**Alotto, R.P.; Codecasa, L.; Freschi, F.; Grusso, G.; Moro, F.; Repetto, M.** (2006): Finite Formulation for Quasi-Magnetostatics with Integral Boundary Conditions. 11<sup>th</sup> *International IGTE Symposium Proceedings*, September 18-20, Graz (Austria), CD form.

**Alotto, R.P.; Grusso, G.; Moro, F.; Repetto, M.** (2008): A Boundary Integral Formulation for Eddy Current Problems Based on the Cell Method. *IEEE Trans. on Magnetics*, vol. 44, pp. 770-773.

**Alotto, R.P.; Perugia I.** (2004): Matrix Properties of a Vector Potential Cell Method for Magnetostatics. *IEEE Trans. on Magnetics*, vol. 40, no. 2, pp. 1045-1048.

**Alshoabi, A.; Hadi, M.; Ariffin, A.** (2007): Two-Dimensional Numerical Estima-

tion of Stress Intensity Factors and Crack Propagation in Linear Elastic Analysis. *J. Struct. Durability Health Monit.*, vol. 3, pp. 15-28.

**Anderson, T.L.** (1991): Fracture Mechanics, Fundamentals and Applications, CRC Press.

**Aour, B.; Rahmani, O.; Nait-Abdelaziz, B.** (2007): A Coupled FEM/BEM Approach and its Accuracy for Solving Crack Problems in Fracture Mechanics. *Int. J. Solids Struct.*, vol. 44., pp. 2523- 2539.

**Bettini, P.; Trevisan, F.** (2003): Electrostatic Analysis for Plane Problems with Finite-formulation. *IEEE Trans. on Magnetics*, vol. 39, no. 3, pp. 1127-1130.

**Bottauscio, O.; Manzin, A.; Canova, A.; Chiampi, M.; Guosso, G.; Repetto, M.** (2004): Field and Circuit Approaches for Diffusion Phenomena in Magnetic Cores. *IEEE Trans. on Magnetics*, vol. 40, no. 2, pp. 1322-1325.

**Bowie, O.L.** (1956): Analysis of an Infinite Plate Containing Radial Cracks originating at the Boundary of an Internal Circular Hole. *J. Math. Phys.*, vol. 35, pp. 60-71.

**Broek, D.** (1974): Elementary Engineering Fracture Mechanics, Nordhoff International Publishing.

**Bullo, M.; D'Ambrosio, V.; Dughiero, F.; Guarnieri, M.** (2006): Coupled Electric and Thermal Transient Conduction Problems with a Quadratic Interpolation Cell Method Approach. *IEEE Trans. on Magnetics*, vol. 42, no. 4, pp. 1003-1006.

**Bullo, M.; D'Ambrosio, V.; Dughiero, F.; Guarnieri, M.** (2007): A 3D Cell Method Formulation for Coupled Electric and Thermal Problems. *IEEE Trans. on Magnetics*, vol. 43, no. 4, pp. 1197-1200.

**Chang, R.** (1981): Static Finite Element Stress Intensity Factors for annular Cracks. *J. Nondestruct. Evaluat.*, vol. 2, pp. 119-124.

**Codecasa, L.; Specogna, R.; Trevisan, F.** (2008): Discrete Constitutive Equations over Hexahedral Grids for Eddy-Current Problems. *CMES: Computer Modeling in Engineering & Sciences*, vol. 31, no. 3, pp. 129-144.

**Cosmi, F.** (2001): Numerical Solution of Plane Elasticity Problems with the Cell Method. *CMES: Computer Modeling in Engineering & Sciences*, vol. 2, no. 3, pp. 365-372.

**Cosmi, F.** (2003): Numerical Modeling of Porous Materials Mechanical Behaviour with the Cell Method. *Proceedings of the Second MIT Conference on Computational Fluid and Solid Mechanics*, Massachusetts Institute of Technology, Cambridge (MA, U.S.A.), pp. 17-20.

**Cosmi, F.** (2005): Elastodynamics with the Cell Method. *CMES: Computer Modeling in Engineering & Sciences*, vol. 8, no. 3, pp. 191-200.

**Cosmi, F.** (2008): Dynamical Analysis of Mechanical Components: a Discrete Model for Damping. *CMES: Computer Modeling in Engineering & Sciences*, vol. 27, no. 3, pp. 187-195.

**Cosmi, F.; Di Marino, F.** (2001): Modelling of the Mechanical Behaviour of Porous Materials: a New Approach. *Acta of Bioengineering and Biomechanics*, vol. 3, no. 2, pp. 55-66.

**Cosmi, F.; Dreossi, D.** (2007): The Application of the Cell Method for the Clinical Assessment of Bone Fracture Risk. *Acta of Bioengineering and Biomechanics*, Wroclaw University of Technology, Wroclaw (Poland), vol. 9, No. 2, pp. 35-39.

**Cosmi, F.; Steimberg, N.; Dreossi, D.; Mazzoleni, G.** (2009): Structural Analysis of Rat Bone Explants in Vitro in Simulated Microgravity Conditions. *J. Mech. Behav. Biomed. Mater.*, vol. 2, no. 2, pp. 164-172.

**De Araújo, T.; Bittencourt, T.; Roehl, D.; Martha, L.** (2000): Numerical Estimation of Fracture Parameters in Elastic and Elastic-Plastic Analysis. *Proceedings of the European Congress on Computational Methods in Applied Sciences and Engineering*, September 11-14, Barcelona (Spain), pp. 1-18.

**Dugdale, D.S.** (1960): Yielding of Steel Sheets Containing Slits. *J. Mech. Phys. Solids*, vol. 8, no. 2, pp. 100-104.

**Erdogan, F.; Sih, G.C.** (1963): On the Extension of Plates under Plane Loading and Transverse Shear. *J. bas. Engng.*, vol. 85, pp. 519-527.

**Ferretti, E.** (2003): Crack Propagation Modeling by Remeshing using the Cell Method (CM). *CMES: Computer Modeling in Engineering & Sciences*, vol. 4, no. 1, pp. 51-72.

**Ferretti, E.** (2004a): A Cell Method (CM) Code for Modeling the Pullout Test Step-wise. *CMES: Computer Modeling in Engineering & Sciences*, vol. 6, no. 5, pp. 453-476.

**Ferretti, E.** (2004b): Experimental Procedure for Verifying Strain-Softening in Concrete. *Int. J. Fract.* (Letters section), vol. 126, no. 2, pp. L27-L34.

**Ferretti, E.** (2004c): Crack-Path Analysis for Brittle and Non-brittle Cracks: a Cell Method Approach. *CMES: Computer Modeling in Engineering & Sciences*, vol. 6, no. 3, pp. 227-244.

**Ferretti, E.** (2005): A Local Strictly Nondecreasing Material Law for Modeling Softening and Size-Effect: a Discrete Approach. *CMES: Computer Modeling in Engineering & Sciences*, vol. 9, no. 1, pp. 19-48.

**Ferretti, E.; Casadio, E.; Di Leo, A.** (2008): Masonry Walls under Shear Test: a CM Modeling. *CMES: Computer Modeling in Engineering & Sciences*, vol. 30, no. 3, pp. 163-190.

- Ferretti, E.; Di Leo, A.** (2003): Modelling of Compressive Tests on FRP Wrapped Concrete Cylinders through a Novel Triaxial Concrete Constitutive Law. *SITA*, vol. 5, pp. 20-43.
- Giuffrida, C.; Gruosso, G.; and Repetto, M.** (2006): Finite Formulation of Non-linear Magnetostatics with Integral Boundary Conditions. *IEEE Trans. on Magnetics*, vol. 42, no. 5, pp. 1503-1511.
- Griffith, A.A.** (1920): The Phenomena of Rupture and Flow in Solids. *Philos. Trans. Roy. Soc. London. Ser. A*, vol. 221, pp. 163-198.
- Gustavo, V.G.; Jaime, P.; Manuel, E.** (2000): KI Evaluation by the Displacement Extrapolation Technique. *Eng. Fract. Mech.*, vol. 66, pp. 243-255.
- Heckel, K.** (1983): Einführung in die technische Anwendung der Bruchmechanik. Carl Hanser Verlag, München.
- Hellen, T.K.** (1975): On the Method of Virtual Crack Extensions. *Int. J. Numer. Methods Eng.*, vol. 9, no. 1, pp. 187-207.
- Heshmatzadeh, M.; Bridges, G.E.** (2007): A Geometrical Comparison between Cell Method and Finite Element Method in Electrostatics. *CMES: Computer Modeling in Engineering & Sciences*, vol. 18, no. 1, pp. 45-58.
- Hussain, M.A.; Pu, S.L.; Underwood, J.H.** (1974): Strain Energy Release Rate for a Crack Under Combined Mode I and Mode II. *Fracture Analysis ASTM STP*, vol. 560, pp. 2-28.
- Hutchinson, J.W.** (1968): Singular Behaviour at the End of a Tensile Crack in a Hardening Material. *J. Mech. Phys. Solids*, vol. 16, pp. 13-31.
- Inglis, C.E.** (1913): Stresses in a Plate due to the Presence of Cracks and Sharp Corners. *Proc. Institute Naval Architects*.
- Irwin, G.R.** (1957): Analysis of Stresses and Strains Near the Ends of a Crack Traversing a Plate. *J. Appl. Mech.*, vol. 24, no. 3, pp. 361-364.
- Irwin, G.R.** (1958): Fracture. In Flügge, S. (Ed.), *Handbuch der Physik*, vol. 6, Springer, Berlin.
- Koenke, C.; Harte, R.; Krätzing, W.B.; Rosenstein, O.** (1998): On adaptive Remeshing Techniques for Crack Simulation Problems. *Eng. Computation*, vol. 15, no. 1, pp. 74-88.
- Kutuka, M.A.; Atmacab, N.; Guzelbey, I.H.** (2007): Explicit Formulation of SIF Using Neural Networks for Opening Mode of Fracture. *Int. J. Eng. Struct.*, vol. 29, pp. 2080-2086.
- Laurencin, J.; Delette, G.; Dupeux, M.** (2007): An Estimation of Ceramic Fracture at Singularities by a Statistical Approach. *J. Eur. Ceramic Soc.*, vol. 28, pp.

1-13.

**Lenov, M.Y.; Panasyuk, V.V.** (1959): Development of Minute Cracks in Solids. *Prikl. Meckhanika*, vol. 5, no. 4, pp. 391-401.

**Marrone, M.** (2004): Properties of Constitutive Matrices for Electrostatic and Magnetostatic Problems. *IEEE Trans. on Magnetics*, vol. 40, no. 3, pp. 1516-1520.

**Marrone, M.; Mitra, R.** (2004): A Theoretical Study of the Stability Criteria for Generalized FDTD Algorithms for Multiscale Analysis. *IEEE Trans. on Antennas and Propagation*, vol. 52, no. 8.

**Marrone, Grassi, P.; M.; Mitra, R.** (2004): A New Technique Based on the Cell Method for Calculation the Propagation Constant of Inhomogeneous Filled Waveguide. *IEEE Trans. on Antennas and Propagation*.

**McClintock, F.** (1958): Ductile Fracture Instability in Shear. *J. Appl. Mech.*, vol. 25, pp. 582-588.

**Murakami, Y.** (1978): A Method of Stress Intensity Factor Calculation for the Crack emanating from an arbitrarily shaped Hole or the Crack in the Vicinity of an arbitrarily shaped Hole. *Trans. Jap. Soc. Mech. Eng.*, vol. 44, pp. 423-432.

**Nappi, A.; Tin-Loi, F.** (2001): A Numerical Model for Masonry Implemented in the Framework of a Discrete Formulation. *Struct. Eng. Mech.*, vol. 11, no. 2, pp. 171-184.

**Newman, J.** (1971): An Improved Method of Collocation for the Stress Analysis of Cracked Plates with various shaped Boundaries. NASA TN., vol. 6376, pp. 1-45.

**Novozhilov, V.V.** (1969): On the Foundations of the Theory of Equilibrium Cracks in Elastic Bodies. *Prikl. Matem. i Mekhan.*, vol. 33, no. 5, pp. 797-812.

**Owen, D.** (1973): Stress Intensity Factors for Cracks in a Plate containing a Hole and in a spinning Disc. *Int. J. Fract.*, vol. 4, pp. 471-476.

**Paris, P.C.; Sih, G.** (1965): Fracture Toughness Testing and its Applications. *In ASTM Special Technical Publication*, no. 381, Philadelphia, pp. 30-81.

**Patron, V.Z.; Morozov, E.M.** (1978): *Elastic-Plastic Fracture Mechanics*. MIR Publishers.

**Rice, J.R.; Rosengren, G.F.** (1968): Plane Stain Deformation near a Crack Tip in a Power-Law Hardening Material. *J. Mech. Phys. Solids*, vol. 16, pp. 1-12.

**Rolfe, S.T.; Barsom, J.M.** (1987): *Fracture and Fatigue Control in Structures, Applications of Fracture Mechanics*, Prentice-Hall, Englewood Cliffs, NJ.

**Shahani, A.; Tabatabaei, S.** (2008): Computation of mixed Mode Stress Intensity

Factors in a Four-Point Bend Specimen. *Applied Meth. Model.*, vol. 32, pp. 1281-1288.

**Sih, G.C.** (1974): Strain Energy Density Factor Applied to Mixed Mode Crack Problems. *Int. J. Fract.*, vol. 10, pp. 321-350.

**Sneddon, I.N.** (1946): The Distribution of Stress in the Neighborhood of a Crack in an Elastic Solid. *Proc. Roy. Soc. London*, vol. A-187, pp. 229-260.

**Souiyah, M.; Muchtar, A.; Alshoaibi, A.; Ariffin. A.K.** (2009): Finite Element Analysis of the Crack Propagation for Solid Mechanics. *Am. J. Applied Sci.*, vol. 6, no. 7. pp. 1396-1402.

**Specogna, R.; Trevisan, F.** (2005): Discrete Constitutive Equations in A- $\chi$  Geometric Eddy-Current Formulation. *IEEE Trans. on Magnetics*, vol. 41, no. 4.

**Stanislav, S.; Zdenek, K.** (2008): Two Parameter Fracture Mechanics: Fatigue Crack Behavior under Mixed Mode Conditions. *Eng. Fract. Mech.*, vol. 75, pp. 857-865.

**Straface, S.; Troisi, S.; Gagliardi, V.** (2006): Application of the Cell Method to the Simulation of Unsaturated Flow. *CMC: Computers, Materials and Continua*, vol. 3, no. 3, pp. 155-166.

**Taddei, F.; Pani, M.; Zovatto, L.; Tonti, E.; Viceconti, M.** (2008): A New Meshless Approach for Subject-Specific Strain Prediction in Long Bones: Evaluation of Accuracy. *Clin. Biomech.*, vol. 23, no. 9, pp. 1192-1199.

**Tonti, E.** (2001a): A Direct Discrete Formulation of Field Laws: the Cell Method. *CMES: Computer Modeling in Engineering & Sciences*, vol. 2, no. 2, pp. 237-258.

**Tonti, E.** (2001b): A Direct Discrete Formulation for the Wave Equation. *J. Comput. Acoust.*, 9(4): 1355-1382.

**Tonti, E.; Zarantonello, F.** (2009): Algebraic Formulation of Elastostatics: the Cell Method. *CMES: Computer Modeling in Engineering & Sciences*, vol. 39, no. 3, pp. 201-236.

**Trevisan, F.; Kettunen, L.** (2004): Geometric Interpretation of Discrete Approaches to Solving Magnetostatics. *IEEE Trans. on Magnetics*, vol. 40, no. 2.

**Wells, A.A.** (1961): Unstable Crack Propagation in Metals: Cleavage and Fast Fracture. *Proc. Crack Propagation Symposium*, vol. 1, College of Aeronautics and the Royal Aeronautical Society, Cranfield (England), pp. 210-230.

**Yan, X.** (2006): Cracks emanating from Circular Hole or Square Hole in Rectangular Plate in Tension. *Eng. Fract. Mech.*, vol. 73, pp. 1743-1754.

